Physics Letters B 820 (2021) 136523

Contents lists available at ScienceDirect

Physics Letters B

www.elsevier.com/locate/physletb

^{12}C(e,e'pN) measurements of short range correlations in the tensor-to-scalar interaction transition region

The CLAS Collaboration

I. Korover [a], J.R. Pybus [b], A. Schmidt [c,b], F. Hauenstein [b,d], M. Duer [e], O. Hen [b,*], E. Piasetzky [e], L.B. Weinstein [d], D.W. Higinbotham [f], S. Adhikari [g], K. Adhikari [h], M.J. Amaryan [d], Giovanni Angelini [i], H. Atac [j], L. Barion [k], M. Battaglieri [f,l], A. Beck [b,1], I. Bedlinskiy [m], Fatiha Benmokhtar [n], A. Bianconi [o,p], A.S. Biselli [q,r], S. Boiarinov [f], W.J. Briscoe [i], W.K. Brooks [s,f], D. Bulumulla [d], V.D. Burkert [f], D.S. Carman [f], A. Celentano [l], P. Chatagnon [t], T. Chetry [h], L. Clark [u], B. Clary [v], P.L. Cole [w,x,y], M. Contalbrigo [k], V. Crede [z], R. Cruz-Torres [b], A. D'Angelo [aa,ab], R. De Vita [l], M. Defurne [ac], A. Denniston [b], A. Deur [f], S. Diehl [v], C. Djalali [ad,ae], R. Dupre [t], H. Egiyan [f], M. Ehrhart [af], A. El Alaoui [s], L. El Fassi [h], L. Elouadrhiri [f], P. Eugenio [z], R. Fersch [ag,ah], A. Filippi [ai], T. Forest [x], G. Gavalian [f,aj], F.X. Girod [f], E. Golovatch [ak], R.W. Gothe [ae], K.A. Griffioen [ah], M. Guidal [t], K. Hafidi [af], H. Hakobyan [s,al], N. Harrison [f], M. Hattawy [d], T.B. Hayward [ah], D. Heddle [ag,f], K. Hicks [ad], M. Holtrop [aj], Y. Ilieva [ae,i], D.G. Ireland [u], E.L. Isupov [ak], D. Jenkins [am], H.S. Jo [an], K. Joo [v], S. Joosten [af], D. Keller [ao], M. Khachatryan [d], A. Khanal [g], M. Khandaker [ap,2], A. Kim [v], C.W. Kim [i], F.J. Klein [y], V. Kubarovsky [f,aq], L. Lanza [aa], M. Leali [o,p], P. Lenisa [k,ar], K. Livingston [u], V. Lucherini [as], I.J.D. MacGregor [u], D. Marchand [t], N. Markov [f], L. Marsicano [l], V. Mascagna [at,p,3], B. McKinnon [u], S. Mey-Tal Beck [b,1], T. Mineeva [s], M. Mirazita [as], A. Movsisyan [k], C. Munoz Camacho [t], B. Mustapha [af], P. Nadel-Turonski [f], K. Neupane [ae], G. Niculescu [au], M. Osipenko [l], A.I. Ostrovidov [z], M. Paolone [j], L.L. Pappalardo [k,ar], R. Paremuzyan [aj], E. Pasyuk [f], W. Phelps [ag], O. Pogorelko [m], J.W. Price [av], Y. Prok [d,ao], D. Protopopescu [u], B.A. Raue [g,f], M. Ripani [l], J. Ritman [aw], A. Rizzo [aa,ab], G. Rosner [u], J. Rowley [ad], F. Sabatié [ac], C. Salgado [ap], R.A. Schumacher [r], E.P. Segarra [b], Y.G. Sharabian [f], U. Shrestha [ad], D. Sokhan [u], O. Soto [as], N. Sparveris [j], S. Stepanyan [f], I.I. Strakovsky [i], S. Strauch [ae,i], J.A. Tan [an], N. Tyler [ae], M. Ungaro [f,aq], L. Venturelli [o,p], H. Voskanyan [al], E. Voutier [t], T. Wang [ax], D. Watts [ay], X. Wei [f], M.H. Wood [az,ae], N. Zachariou [ay], J. Zhang [ao], Z.W. Zhao [ba], X. Zheng [ao]

[a] *Nuclear Research Center Negev, Be'er Sheva 84190, Israel*
[b] *Massachusetts Institute of Technology, Cambridge, MA 02139, USA*
[c] *The George Washington University, Washington, DC, 20052, USA*
[d] *Old Dominion University, Norfolk, VA 23529, USA*
[e] *School of Physics and Astronomy, Tel Aviv University, Tel Aviv 69978, Israel*
[f] *Thomas Jefferson National Accelerator Facility, Newport News, VA 23606, USA*
[g] *Florida International University, Miami, FL 33199, USA*
[h] *Mississippi State University, Mississippi State, MS 39762-5167, USA*
[i] *The George Washington University, Washington, DC 20052, USA*

* Corresponding author.
E-mail address: hen@mit.edu (O. Hen).
[1] On sabbatical leave from Nuclear Research Center Negev, Be'er Sheva 84190, Israel.
[2] Current address: Idaho State University, Pocatello, Idaho 83209.
[3] Current address: Università degli Studi di Brescia, 25123 Brescia, Italy.

https://doi.org/10.1016/j.physletb.2021.136523

[j] Temple University, Philadelphia, PA 19122, USA
[k] INFN, Sezione di Ferrara, 44100 Ferrara, Italy
[l] INFN, Sezione di Genova, 16146 Genova, Italy
[m] National Research Centre Kurchatov Institute - ITEP, Moscow, 117259, Russia
[n] Duquesne University, 600 Forbes Avenue, Pittsburgh, PA 15282, USA
[o] Università degli Studi di Brescia, 25123 Brescia, Italy
[p] INFN, Sezione di Pavia, 27100 Pavia, Italy
[q] Fairfield University, Fairfield CT 06824, USA
[r] Carnegie Mellon University, Pittsburgh, PA 15213, USA
[s] Universidad Técnica Federico Santa María, Casilla 110-V, Valparaíso, Chile
[t] Universit'e Paris-Saclay, CNRS/IN2P3, IJCLab, 91405 Orsay, France
[u] University of Glasgow, Glasgow G12 8QQ, United Kingdom
[v] University of Connecticut, Storrs, CT 06269, USA
[w] Lamar University, 4400 MLK Blvd, PO Box 10009, Beaumont, TX 77710, USA
[x] Idaho State University, Pocatello, ID 83209, USA
[y] Catholic University of America, Washington, D.C. 20064, USA
[z] Florida State University, Tallahassee, FL 32306, USA
[aa] INFN, Sezione di Roma Tor Vergata, 00133 Rome, Italy
[ab] Universita' di Roma Tor Vergata, 00133 Rome, Italy
[ac] IRFU, CEA, Université Paris-Saclay, F-91191 Gif-sur-Yvette, France
[ad] Ohio University, Athens, OH 45701, USA
[ae] University of South Carolina, Columbia, SC 29208, USA
[af] Argonne National Laboratory, Argonne, IL 60439, USA
[ag] Christopher Newport University, Newport News, VA 23606, USA
[ah] College of William and Mary, Williamsburg, VA 23187-8795, USA
[ai] INFN, Sezione di Torino, 10125 Torino, Italy
[aj] University of New Hampshire, Durham, NH 03824-3568, USA
[ak] Skobeltsyn Institute of Nuclear Physics, Lomonosov Moscow State University, 119234 Moscow, Russia
[al] Yerevan Physics Institute, 375036 Yerevan, Armenia
[am] Virginia Tech, Blacksburg, VA 24061-0435, USA
[an] Kyungpook National University, Daegu 41566, Republic of Korea
[ao] University of Virginia, Charlottesville, VA 22901, USA
[ap] Norfolk State University, Norfolk, VA 23504, USA
[aq] Rensselaer Polytechnic Institute, Troy, NY 12180-3590, USA
[ar] Universita' di Ferrara, 44121 Ferrara, Italy
[as] INFN, Laboratori Nazionali di Frascati, 00044 Frascati, Italy
[at] Università degli Studi dell'Insubria, 22100 Como, Italy
[au] James Madison University, Harrisonburg, VA 22807, USA
[av] California State University, Dominguez Hills, Carson, CA 90747, USA
[aw] Institute fur Kernphysik (Juelich), Juelich, Germany
[ax] School of Physics, Beihang University, Beijing 100191, China
[ay] University of York, York YO10 5DD, United Kingdom
[az] Canisius College, Buffalo, NY, USA
[ba] Duke University, Durham, NC 27708-0305, USA

ARTICLE INFO

Article history:
Received 4 February 2021
Received in revised form 13 July 2021
Accepted 13 July 2021
Available online 28 July 2021
Editor: D.F. Geesaman

ABSTRACT

High-momentum configurations of nucleon pairs at short-distance are probed using measurements of the $^{12}C(e,e'p)$ and $^{12}C(e,e'pN)$ reactions (where N is either n or p), at high-Q^2 and $x_B > 1.1$. The data span a missing-momentum range of 300–1000 MeV/c and are predominantly sensitive to the transition region of the strong nuclear interaction from a Tensor to Scalar interaction. The data are well reproduced by theoretical calculations using the Generalized Contact Formalism with both chiral and phenomenological nucleon-nucleon (NN) interaction models. This agreement suggests that the measured high missing-momentum protons up to 1000 MeV/c predominantly belong to short-ranged correlated (SRC) pairs. The measured $^{12}C(e,e'pN)$ / $^{12}C(e,e'p)$ and $^{12}C(e,e'pp)$ / $^{12}C(e,e'pn)$ cross-section ratios are consistent with a decrease in the fraction of proton-neutron SRC pairs and increase in the fraction of proton-proton SRC pairs with increasing missing momentum. This confirms the transition from an isospin-dependent tensor NN interaction at $\sim$ 400 MeV/c to an isospin-independent scalar interaction at high-momentum around $\sim$ 800 MeV/c as predicted by theoretical calculation.

High momentum-transfer electron- and proton-scattering measurements, as well as many-body *ab-initio* calculations, have shown that nucleons in the nuclear ground state temporarily form pairs with large relative momentum and smaller center-of-mass (CM) momentum. These are called Short-Range Correlated (SRC) pairs [1,2]. The existence and characteristics of SRC pairs are related to outstanding issues in particle, nuclear, and astrophysics, including the modification of the internal structure of nucleons bound in atomic nuclei (i.e., the EMC effect) [2–6], matrix elements used to interpret searches for neutrinoless double beta decay [7–10], scale separation and factorization of many-body nuclear wavefunctions [1,11–14], nuclear charge radii [15], and the nuclear symmetry energy governing neutron star properties [16–18].

A well-established feature of SRC pairs is their predominance by proton-neutron (pn) pairs in the missing momentum range of 300–600 MeV/c [19–22]. This results from the preference for spin-1 pn-pairs by the tensor part of the NN interaction, which dominates over the scalar part of the interaction at these missing momenta [23–25]. At higher missing momentum calculations suggest that the scalar repulsive core should become dominant and

lead to an increased fraction of proton-proton (pp) SRC pairs [1,2,12,26,27]. SRC measurements of this tensor-to-scalar transition provide valuable insight into the nature of the strong nuclear interaction at short-distances.

The tensor-to-scalar transition was studied experimentally in two previous works via measurements of the relative abundances of pn- and pp-SRC, extracted from $(e,e'pp)$ / $(e,e'pn)$ and $(e,e'pN)$ / $(e,e'p)$ cross-section ratios (where N is either n or p). Ref. [28] measured the missing momentum dependence of these cross-section ratios in ^{4}He out to 800 MeV/c. The measured $^4\mathrm{He}(e,e'pp)$ / $^4\mathrm{He}(e,e'pn)$ ratio was consistent with the expected increase in the pp-SRC fraction with increased momenta. However, the data has large uncertainties and the suggested increase was due to an underlying decrease in the $^4\mathrm{He}(e,e'pn)$ / $^4\mathrm{He}(e,e'p)$ ratio (i.e. less np-SRC pairs), whereas the $^4\mathrm{He}(e,e'pp)$ / $^4\mathrm{He}(e,e'p)$ ratio was overall flat as a function of missing momentum (i.e. no increase in pp-SRC pairs).

More recently Ref. [29] measured the $^{12}\mathrm{C}(e,e'pp)$ / $^{12}\mathrm{C}(e,e'p)$ reaction yield ratio over the missing-momentum range of 400 to 1000 GeV/c, observing a clear increase as a function of missing momentum. This measurement had significantly improved kinematics compared with Ref. [28], reaching $\langle Q^2\rangle \sim$ 3–3.5 GeV/c^2 for large missing momentum. However, it was limited by only measuring the $^{12}\mathrm{C}(e,e'pp)$ / $^{12}\mathrm{C}(e,e'p)$ reaction yield ratio. This makes its interpretation subject to several theoretical assumptions that the data itself cannot verify. These include the assumptions that (a) all high missing-momentum protons belonged to 2N-SRC pairs, and (b) reaction effects were properly accounted for, primarily (n,p) single-charge exchange (SCX) processes. As np-SRC are always more abundant than pp-SRCs, even a modest SCX probability can significantly distort the $(e,e'pp)$ reaction by having a large number of observed $(e,e'pp)$ events originating from interactions with pn-SRC pairs in which the neutron undergoes SCX. The impact of SCX on the data of Ref. [29] can be as large as 400%, with a large missing-momentum dependence (see supplementary materials Fig. S36). Thus, while experimentally simpler to measure, SRC studies via the $(e,e'pp)$ reaction are subject to model-dependent assumptions and corrections that have not yet been tested experimentally.

Here we present the results of a direct simultaneous measurement of pn- and pp-SRC pairs using the $^{12}\mathrm{C}(e,e'pN)$ and $^{12}\mathrm{C}(e,e'p)$ reactions. The $^{12}\mathrm{C}(e,e'pn)$ data are minimally sensitive to SCX corrections due to the small fraction of initial-state pp-SRC pairs, but have larger uncertainties due to the low neutron detection efficiency, particularly for the lower momentum neutrons of the lower missing momentum data. The $^{12}\mathrm{C}(e,e'pp)$ data are more precise but sensitive to SCX corrections. Together, the measurement of the different reaction channels, in combination with theoretical calculations using the Generalized Contact Formalism (GCF) [13,14,30,31], allow establishing the 2N-SRC dominance of the measured reactions and the observation of a scalar repulsive interaction at short distances.

The analysis reported on herein is based on data collected in 2004 in Hall B of the Thomas Jefferson National Accelerator Facility (Jefferson Lab) in Virginia, USA, re-analyzed here as part of the Jefferson Lab data-mining initiative [32]. This data comes from measurements of 5.01 GeV electrons scattered from deuterium and carbon targets [33], detecting the scattered electrons, knocked-out protons, and recoil neutrons in the CEBAF Large Acceptance Spectrometer (CLAS) [34].

CLAS utilized a toroidal magnetic field and six independent sets of drift chambers (DCs) [35], time-of-flight (TOF) scintillation counters [36], Cherenkov counters (CCs) [37], and electromagnetic calorimeters (EC) [38] for charged particle detection and identification. Charged particle momenta were inferred from their reconstructed trajectories within the magnetic field. Electrons were identified by requiring a signal in the CC, as well as a characteristic energy deposition in the EC. Protons were identified through correlations between momentum and flight time. The TOF and DC polar angular acceptance was $8^\circ \le \theta \le 140^\circ$ and the azimuthal angular acceptance ranged from 50% at small polar angles to 80% at larger polar angles. The EC and CC polar angular acceptance was limited to $< 45^\circ$.

Neutrons with momenta of 200–1000 MeV/c were detected in the TOF counters by requiring a hit with energy deposition above threshold (nominally 8 MeV electron equivalent, or MeVee), no matching charged-particle track (or partial track) in the drift chambers, and a TOF that corresponded to $\beta < 0.75$. We only considered hits reconstructed inside a fiducial region that excluded 10 cm from the ends of all scintillator paddles. Our results are not sensitive to the exact exclusion region. Neutron momenta were determined by time-of-flight, with a typical resolution of 25–40 MeV/c. This is the first work to measure recoil neutrons in CLAS.

The neutron detection efficiency was determined using the over-constrained $d(e,e'p)n$ and $d(e,e'pn)$ reactions. The efficiency was extracted for different TOF energy deposition thresholds in the range of 4–10 MeV electron-equivalent (MeVee, i.e., events where the neutron-induced signal measured in the TOF bar is higher than that produced by an electron that deposited 4–10 MeV in that bar), and as a function of the recoil neutron momentum determined by the $d(e,e'p)n$ reaction. For momenta above 400 MeV/c, the typical efficiency was 4–5%. Between 200 and 400 MeV/c, the efficiency was somewhat lower, approximately 2–3%. We verified that the charged-particle veto efficiency, using the DC tracking system, resulted in a negligible fraction of charged particles mis-identified as neutrons due to tracking inefficiencies. Measured neutron yields are always shown after efficiency corrections. See online supplementary materials for additional details on the neutron identification, detection efficiency, and momentum reconstruction resolution.

Similar to previous SRC studies [20,21,29,39,40], we considered events with scattered electron kinematics of four momentum transfer squared $Q^2 \equiv |\vec{q}|^2 - \omega^2 > 1.5$ GeV^2/c^2 and Bjorken scaling variable $x_B \equiv Q^2/2m_N\omega > 1.1$, where m_N is the nucleon mass, while $\vec{q}$ and ω are the 3-momentum and energy transferred to the nucleus by the electron, respectively. Assuming the electron scatters from a single nucleon that does not reinteract as it leaves the nucleus with momentum $\vec{p}_f$, the initial nucleon momentum $\vec{p}_i$ can be approximated as equal to the measured missing-momentum: $\vec{p}_i \approx \vec{p}_{\mathrm{miss}} \equiv \vec{p}_f - \vec{q}$. We select $300 < p_{\mathrm{miss}} < 1000$ MeV/c to enhance contributions from interactions with high initial momentum nucleons, and require an angle between $\vec{p}_f$ and $\vec{q}$ smaller than 25°, $0.62 < |\vec{p}_f|/|\vec{q}| < 0.96$ to select leading nucleons. Resonance production is suppressed by requiring that the $(e,e'p)$ reaction missing mass, assuming scattering off a standing nucleon pair, will be smaller than the sum of the nucleon and pion mass, i.e. $M_{\mathrm{miss}} \equiv \sqrt{(q^\mu - p_f^\mu + 2m_N)^2} < 1.1$ GeV/c^2.

If the struck nucleon is part of a 2N-SRC pair, we interpret the reaction through the SRC break-up model where a correlated partner nucleon is assumed to exist as an on-shell spectator carrying momentum $\vec{p}_{\mathrm{recoil}}$. Triple coincidence $^{12}\mathrm{C}(e,e'pN)$ events were selected from the $^{12}\mathrm{C}(e,e'p)$ event sample by requiring the coincidence detection of such a recoil nucleon (proton or neutron) in CLAS with momentum $350 < p_{\mathrm{recoil}} < 1000$ MeV/c. For neutron recoils, the neutron arrival time spectrum at the scintillators has a peak corresponding to the neutron events sitting on top of a similar-size uncorrelated random background. This background is uniform in hit time, allowing it to be estimated from off-time neutrons and subtracted. More details on the event selection and background subtraction can be found in the online supplementary materials.

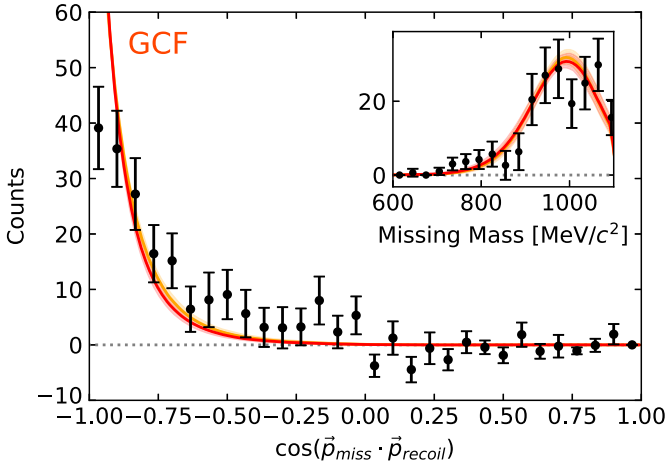

Fig. 1. Background-subtracted angular correlation between the reconstructed $(e, e'p)$ missing momentum vector ($\vec{p}_{\rm miss}$) and recoil neutron momentum vector ($\vec{p}_{\rm recoil}$), for data events passing ^{12}C$(e, e'pn)$ cuts (points), compared with GCF predictions based on the AV18 and N2LO *NN* interactions (darker and lighter bands, respectively). Insert shows the background-subtracted missing mass distribution for the same events and calculation. The width of the bands corresponds to the 68% confidence interval due to uncertainties in the model parameters.

The $x_B > 1.1$ selection is consistent with that used in Refs. [19,21,28,39,41] and is slightly lower than the $x_B > 1.2$ selection used by Refs. [20,29,40]. The lower cut value is chosen to increase statistics; we verified that this change does not impact our agreement with the published $(e, e'pp)$ / $(e, e'p)$ ratio of Ref. [29] that used $x_B > 1.2$ (supplementary materials Fig. S27).

Fig. 1 shows the cosine of the angle between $\vec{p}_{\rm miss}$ and the "recoil" neutron momentum $\vec{p}_{\rm recoil}$ for ^{12}C$(e, e'pn)$ events, after random coincidence background subtraction. While the recoil neutron selection criteria do not place any angular requirements, the measured distribution shows a clear back-to-back correlation characteristic of SRC breakup events.

The measured distributions show good agreement with theoretical predictions based on the GCF [13,14,30,31] using both the AV18 [42] and N2LO(1.0) [43] *NN* interaction models.

The GCF assumes scale-separation between the short-distance interactions within an SRC pair, and the long-range interactions between the pair and the rest of the nucleus, as well as their mutual separation from the ultra-short distance scale associated with the high-energy virtual photon probe. With this in mind, Ref. [30] suggested a factorized approximation for the correlated continuum region of the nuclear spectral function, that can be used in factorized models of the scattering cross-section at large momentum transfer kinematic [44]. Here the hard break-up of an SRC pair is assumed to proceeds via a reaction in which the virtual photon is absorbed by a single nucleon in an SRC pair, knocking it out of the nucleus and leaving its correlated partner nucleon to recoil from the nucleus [30,31].

For completeness we note that beyond the use of the specific GCF model for the spectral function, the reaction model used herein adopts a high-resolution theoretical description of high-momentum transfer reactions where the reaction is modeled using one-body operators and correlation effects are embedded in the nuclear wave function. While constituting a valid simple reaction picture that is consistent with both data and various ab initio calculations, it is not the only possible description of our data. Unitary freedom allows shifting the explicit effects of two-body correlations from nuclear wave functions to the interaction operators while keeping the calculated cross-section invariant [45]. Thus, theoretical studies can also use our data to study complementary factorized models [26] and/or constrain many-body reaction operators used in low-resolution nuclear theory calculations.

Several ingredients are necessary to construct the GCF based factorized cross-section [31]. We used the off-shell electron-nucleon cross-section from Ref. [46]. Nuclear contacts [13,14,30], and the possible excitation range of the residual $A-2$ nuclear system E^* are the same as in Ref. [29]. The pair CM momentum distribution is assumed to be a three-dimensional Gaussian [11,47] with a characteristic width taken from Ref. [40]. Additionally, we accounted for Final State Interactions (FSIs) including Single Charge Exchange (SCX) and nuclear transparency using the Glauber approximation from Ref. [48]. The transparency correction is a simple overall scale factor and was previously shown to well-reproduce experimental data [49–51]. However, the SCX corrections affect the missing-momentum dependence of the data, are less certain, and were not validated experimentally. Therefore, obtaining a consistent picture from analysis of both $(e, e'pn)$ and $(e, e'pp)$ data with minimal and maximal SCX sensitivity, respectively, is crucial for a reliable interpretation of experimental data.

Systematic model uncertainties associated with the GCF predictions were estimated by repeating the theoretical calculations with randomly sampled model parameters from a distribution centered around the parameter's nominal value with a width defined by its uncertainty. We also considered two different prescriptions for the off-shell electron-nucleon cross-section known as cc1 and cc2 from Ref. [46].

Supplementary materials Fig. S35 shows comparisons between the GCF calculations and the measured $p_{\rm miss}$-dependence of the ^{12}C$(e, e'pn)$ / ^{12}C$(e, e'p)$, ^{12}C$(e, e'pp)$ / ^{12}C$(e, e'p)$ and ^{12}C$(e, e'pp)$ / ^{12}C$(e, e'pn)$ yield ratios. The data are corrected for nuclear transparency. Since this correction has no $p_{\rm miss}$-dependence, it only changes the overall scale. The data and calculations are in good agreement.

To extract cross-section ratios from the ratios of measured event yields, we corrected for SCX effects, nuclear transparency, experimental acceptance, and the efficiency of the event selection criteria. These corrections were determined by comparing the GCF cross-section to a detailed Monte Carlo simulation that used the GCF cross-section as input. Simulated events were propagated through a model of the CLAS detector that included acceptance, efficiency, and resolution effects, and were then required to pass the exact same event selection criteria. The detector and detector+SCX correction factors are shown in supplementary materials Fig. S36. Further details can be found in Ref. [31].

The uncertainty on the acceptance correction combined the systematic uncertainty of the GCF model, described above, with uncertainty on the acceptance coming from limited knowledge of the spectrometer momentum resolution. This was treated by varying the detector model's momentum resolutions for electrons, protons, and neutrons within uncertainties in the same manner as the GCF model parameters.

Fig. 2 shows the resulting ^{12}C$(e, e'pn)$ / ^{12}C$(e, e'p)$, ^{12}C$(e, e'pp)$ / ^{12}C$(e, e'p)$, and ^{12}C$(e, e'pp)/2$ / ^{12}C$(e, e'pn)$ cross-section ratios as a function of $p_{\rm miss}$. The data are compared with GCF calculations. For $p_{\rm miss} > 400$ MeV/c the calculations agree well with the measured data for either *NN* potential. This agreement supports the validity of the GCF description of the nuclear ground state at high-momentum. For $300 < p_{\rm miss} < 400$ MeV/c, especially for the ^{12}C$(e, e'pp)/2$ / ^{12}C$(e, e'pn)$ ratio, the AV18 calculation agrees well with the data but the N2LO calculation does not. This missing-momentum region is most sensitive to the details of the dip in the *pp* wave function which is absent for spin-1 *pn* pairs due to the tensor interaction [23–25]. This dip has slightly different characteristics for AV18 and N2LO, possibly owing to the N2LO interaction's short-distance regulator [14]. On the other hand the GCF is an

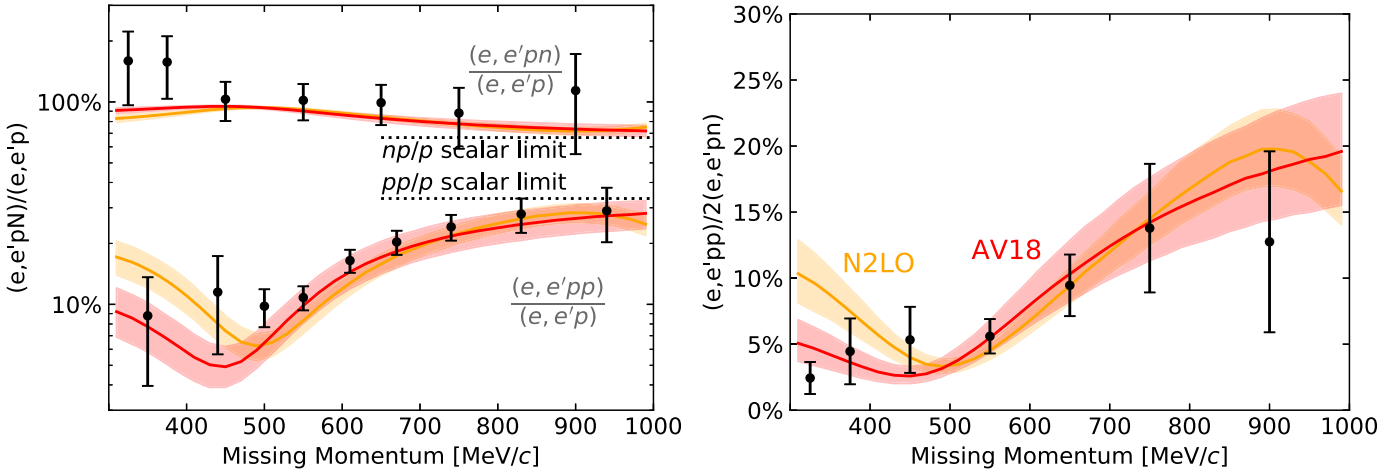

Fig. 2. Left: The measured $C(e,e'pp)$ / $C(e,e'p)$ and $C(e,e'pn)$ / $C(e,e'p)$ cross-section ratios (points), compared with GCF predictions using the AV18 (darker band) and N2LO (light band) NN interaction models. Right: the measured $C(e,e'pp)/2$ / $C(e,e'pn)$ cross-section ratio (points), compared with GCF predictions using the AV18 (darker) and N2LO (lighter) NN interaction models. In both panels, all cross-section ratios were corrected for experimental effects (detector acceptance, efficiency, and resolution) as well as reaction effects including transparency flux lost and SCX. The dashed lines mark the scalar limit obtained from a simple nucleon counting, see text for details. The width of the GCF calculation bands shows their 68% confidence interval due to uncertainties on the model parameters. The data error bars show the quadratic sum of the statistical uncertainty and systematic uncertainty associated with the correction of experimental effects (see online supplementary materials for details on the uncertainty estimation). Not shown are the normalization uncertainties on the data; the $C(e,e'pp)$ / $C(e,e'p)$ and $C(e,e'pn)$ / $C(e,e'p)$ data include a 5% uncertainty resulting from transparency corrections, and the $C(e,e'pn)$ data include correlated systematic uncertainties as listed in Table S3.

asymptotic model and the observed discrepancy appears near the lower edge of its applicability [13,14] and should thus be studied in greater detail by future works. At the highest missing momenta the data agree with the scalar limit prediction where the number of spin-1 pn SRC pairs should be three times the number of spin-0 pp, pn and nn pairs, owing to the three possible spin orientations.

Last, Fig. 3 shows the fraction of $(e,e'p)$ events with a correlated recoil nucleon, i.e., the $[^{12}C(e,e'pp) + {}^{12}C(e,e'pn)]$ / $^{12}C(e,e'p)$ cross-section ratio. Unlike the individual $^{12}C(e,e'pN)$ / $^{12}C(e,e'p)$ ratios, this sum is insensitive to SCX corrections. The data show no significant missing-momentum dependence and imply that within uncertainties, all high-initial-momentum protons are accompanied by a correlated spectator recoil nucleon and therefore belong to a 2N-SRC. The mean of the data points exceeds 100%. This is consistent given the large correlated normalization uncertainty of approximately 12% that is driven by uncertainties in the neutron detection efficiency and transparency correction that will both take all data points up or down and thus can lead to an 'unphysical' mean value for the data (see supplementary materials for details). At the 95% confidence level the data exclude contributions from sources other than 2N-SRCs above 11%. This bound is determined while accounting for both data statistical and systematic uncertainties, with the latter including both point-to-point and correlated normalization uncertainties.

To conclude, we report on new measurements of the $^{12}C(e,e'pn)$ reaction, and improved measurements of the $^{12}C(e,e'pp)$ and $^{12}C(e,e'p)$ reactions at very high missing momentum. The data are used to study the evolution of the isospin dependence of NN-SRCs via the $C(e,e'pp)/2$ / $C(e,e'pn)$ cross-section ratio, and the dominance of high-momentum nucleons by 2N-SRC pairs via the $(e,e'pn)$ / $(e,e'p)$ and $(e,e'pp)$ / $(e,e'p)$ cross-section ratios and their sum. The data are compared with GCF calculations using the AV18 and N2LO interactions. The data agrees with both calculations for $p_{miss} > 400$ MeV/c, but disagrees with the N2LO-based calculation for $300 < p_{miss} < 400$ MeV/c, near the lower edge of the applicability of the GCF [13,14].

The overall good agreement of the GCF calculation with both $^{12}C(e,e'pn)$ and $^{12}C(e,e'pp)$ data indicates that, within the uncertainty of the data, the measured reactions are dominated by interactions with NN-SRC pairs and that reaction effects such as SCX,

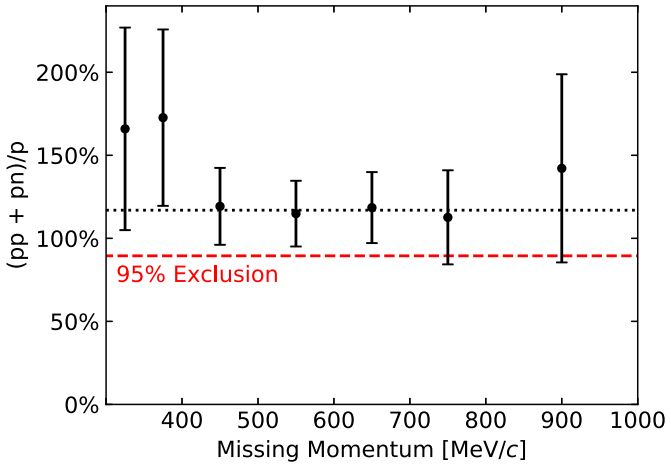

Fig. 3. The fraction of high-momentum protons with a measured recoil partner nucleon for ^{12}C: the measured ratio of $(e,e'pp) + (e,e'pn)$ events to $(e,e'p)$ events as a function of $\vec{p}_{miss}$. The dotted (black) line is the best constant fit 117%. The dashed (red) line shows the 95% CL lower bound on the 2N-SRC contribution to the $^{12}C(e,e'p)$ strength in the measured missing-momentum range at 89%.

which has a large impact on the $^{12}C(e,e'pp)$ channel but a small impact on the $^{12}C(e,e'pn)$ channel, are sufficiently well modeled.

The combination of all data and calculations confirms the observation of a transition of the NN interaction from a tensor-dominated region around relative momenta of 400 MeV/c to a predominantly scalar interaction around 800 MeV/c, validating the use of the NN interactions examined here at high-momentum/short distance regimes. Future extensions of the GCF to three-nucleon correlations as well as forthcoming measurements [52] of three-nucleon knockout reactions $A(e,e'pNN)$ will allow similar studies of the short-distance three-body interactions that are needed for a complete description of neutron stars [53].

Declaration of competing interest

The authors declare that they have no known competing financial interests or personal relationships that could have appeared to influence the work reported in this paper.

Acknowledgements

We acknowledge the efforts of the staff of the Accelerator and Physics Divisions at Jefferson Lab that made this experiment possible. The analysis presented here was carried out as part of the Jefferson Lab Hall B Data-Mining project supported by the U.S. Department of Energy (DOE). The research was also supported by the National Science Foundation, the PAZY Foundation, the Israel Science Foundation and the United Kingdom's Science and Technology Facilities Council (STFC). The Jefferson Science Associates operates the Thomas Jefferson National Accelerator Facility for the DOE, Office of Science, Office of Nuclear Physics under Contract No. DE-AC05-06OR23177.

Appendix A. Supplementary material

Supplementary material related to this article can be found online at https://doi.org/10.1016/j.physletb.2021.136523.

References

[1] C. Ciofi degli Atti, Phys. Rep. 590 (2015) 1.
[2] O. Hen, G.A. Miller, E. Piasetzky, L.B. Weinstein, Rev. Mod. Phys. 89 (2017) 045002.
[3] L.B. Weinstein, E. Piasetzky, D.W. Higinbotham, J. Gomez, O. Hen, R. Shneor, Phys. Rev. Lett. 106 (2011) 052301.
[4] B. Schmookler, et al., CLAS Collaboration, Nature 566 (2019) 354.
[5] G.A. Miller, Phys. Rev. Lett. 123 (2019) 232003, arXiv:1907.00110 [nucl-th].
[6] E.P. Segarra, A. Schmidt, T. Kutz, D.W. Higinbotham, E. Piasetzky, M. Strikman, L.B. Weinstein, O. Hen, Phys. Rev. Lett. 124 (2020) 092002.
[7] M. Kortelainen, J. Suhonen, Phys. Rev. C 75 (2007) 051303, arXiv:0705.0469 [nucl-th].
[8] F. Simkovic, A. Faessler, H. Muther, V. Rodin, M. Stauf, Phys. Rev. C 79 (2009) 055501, arXiv:0902.0331 [nucl-th].
[9] O. Benhar, R. Biondi, E. Speranza, Phys. Rev. C 90 (2014) 065504, arXiv:1401.2030 [nucl-th].
[10] R. Cruz-Torres, A. Schmidt, G.A. Miller, L.B. Weinstein, N. Barnea, R. Weiss, E. Piasetzky, O. Hen, Phys. Lett. B 785 (2018) 304, arXiv:1710.07966 [nucl-th].
[11] C. Ciofi degli Atti, S. Simula, Phys. Rev. C 53 (1996) 1689.
[12] H. Feldmeier, W. Horiuchi, T. Neff, Y. Suzuki, Phys. Rev. C 84 (2011) 054003, arXiv:1107.4956 [nucl-th].
[13] R. Weiss, R. Cruz-Torres, N. Barnea, E. Piasetzky, O. Hen, Phys. Lett. B 780 (2018) 211.
[14] R. Cruz-Torres, D. Lonardoni, R. Weiss, N. Barnea, D.W. Higinbotham, E. Piasetzky, A. Schmidt, L.B. Weinstein, R.B. Wiringa, O. Hen, Nat. Phys. 17 (2020) 306, arXiv:1907.03658 [nucl-th].
[15] G.A. Miller, A. Beck, S. May-Tal Beck, L.B. Weinstein, E. Piasetzky, O. Hen, Phys. Lett. B 793 (2019) 360, arXiv:1805.12099 [nucl-th].
[16] B.-A. Li, B.-J. Cai, L.-W. Chen, J. Xu, Prog. Part. Nucl. Phys. 99 (2018) 29, arXiv:1801.01213 [nucl-th].
[17] O. Hen, B.-A. Li, W.-J. Guo, L.B. Weinstein, E. Piasetzky, Phys. Rev. C 91 (2015) 025803.
[18] L. Frankfurt, M. Sargsian, M. Strikman, Int. J. Mod. Phys. A 23 (2008) 2991, arXiv:0806.4412 [nucl-th].
[19] R. Subedi, et al., Science 320 (2008) 1476, arXiv:0908.1514 [nucl-ex].
[20] O. Hen, et al., Science 346 (2014) 614, arXiv:1412.0138 [nucl-ex].
[21] M. Duer, et al., CLAS Collaboration, Phys. Rev. Lett. 122 (2019) 172502, arXiv:1810.05343 [nucl-ex].
[22] E. Piasetzky, M. Sargsian, L. Frankfurt, M. Strikman, J.W. Watson, Phys. Rev. Lett. 97 (2006) 162504.
[23] R. Schiavilla, R.B. Wiringa, S.C. Pieper, J. Carlson, Phys. Rev. Lett. 98 (2007) 132501.
[24] M. Alvioli, C.C. degli Atti, H. Morita, Phys. Rev. Lett. 100 (2008) 162503.
[25] M.M. Sargsian, T.V. Abrahamyan, M.I. Strikman, L.L. Frankfurt, Phys. Rev. C 71 (2005) 044615.
[26] J. Ryckebusch, W. Cosyn, S. Stevens, C. Casert, J. Nys, Phys. Lett. B 792 (2019) 21, arXiv:1808.09859 [nucl-th].
[27] M. Lyu, T. Myo, H. Toki, H. Horiuchi, C. Xu, N. Wan, Phys. Lett. B 805 (2020) 135421, arXiv:1912.10288 [nucl-th].
[28] I. Korover, N. Muangma, O. Hen, et al., Phys. Rev. Lett. 113 (2014) 022501.
[29] A. Schmidt, et al., CLAS, Nature 578 (2020) 540, arXiv:2004.11221 [nucl-ex].
[30] R. Weiss, I. Korover, E. Piasetzky, O. Hen, N. Barnea, Phys. Lett. B 791 (2019) 242, arXiv:1806.10217 [nucl-th].
[31] J. Pybus, I. Korover, R. Weiss, A. Schmidt, N. Barnea, D. Higinbotham, E. Piasetzky, M. Strikman, L. Weinstein, O. Hen, Phys. Lett. B 805 (2020) 135429, arXiv:2003.02318 [nucl-th].
[32] L. Weinstein, S. Kuhn, 2016, DOE Grant dE-SC0006801.
[33] H. Hakobyan, et al., Nucl. Instrum. Methods Phys. Res., Sect. A 592 (2008) 218.
[34] B.A. Mecking, et al., Nucl. Instrum. Methods Phys. Res., Sect. A 503 (2003) 513.
[35] M.D. Mestayer, et al., Nucl. Instrum. Methods Phys. Res., Sect. A 449 (2000) 81.
[36] E.S. Smith, et al., Nucl. Instrum. Methods Phys. Res., Sect. A 432 (1999) 265.
[37] G. Adams, et al., Nucl. Instrum. Methods Phys. Res., Sect. A 465 (2001) 414.
[38] M. Amarian, et al., Nucl. Instrum. Methods Phys. Res., Sect. A 460 (2001) 239.
[39] M. Duer, et al., CLAS Collaboration, Nature 560 (2018) 617.
[40] E.O. Cohen, et al., CLAS Collaboration, Phys. Rev. Lett. 121 (2018) 092501, arXiv:1805.01981 [nucl-ex].
[41] R. Shneor, et al., Jefferson Lab Hall, Phys. Rev. Lett. 99 (2007) 072501, arXiv:nucl-ex/0703023.
[42] R.B. Wiringa, V.G.J. Stoks, R. Schiavilla, Phys. Rev. C 51 (1995) 38.
[43] A. Gezerlis, I. Tews, E. Epelbaum, S. Gandolfi, K. Hebeler, A. Nogga, A. Schwenk, Phys. Rev. Lett. 111 (2013) 032501, arXiv:1303.6243 [nucl-th].
[44] J. Kelly, Adv. Nucl. Phys. 23 (1996) 75.
[45] S.N. More, S.K. Bogner, R.J. Furnstahl, Phys. Rev. C 96 (2017) 054004, arXiv:1708.03315 [nucl-th].
[46] T. De Forest, Nucl. Phys. A 392 (1983) 232.
[47] C. Colle, W. Cosyn, J. Ryckebusch, M. Vanhalst, Phys. Rev. C 89 (2014) 024603.
[48] C. Colle, W. Cosyn, J. Ryckebusch, Phys. Rev. C 93 (2016) 034608.
[49] O. Hen, et al., CLAS Collaboration, Phys. Lett. B 722 (2013) 63.
[50] C. Colle, et al., Phys. Rev. C 92 (2015) 024604.
[51] M. Duer, et al., CLAS Collaboration, Phys. Lett. B 797 (2019) 134792, arXiv:1811.01823 [nucl-ex].
[52] O. Hen, et al., 2018, Jefferson Lab approved experiment E12-17-006A.
[53] S. Gandolfi, J. Carlson, S. Reddy, Phys. Rev. C 85 (2012) 032801, arXiv:1101.1921 [nucl-th].